

# Application and Analyses of Dynamic Reconfiguration Manipulability Shape Index into Humanoid Biped Walking

Keli Shen<sup>1</sup>, Xiang Li, Hongzhi Tian, Daiji Izawa and Mamoru Minami, Takayuki Matsuno

**Abstract**—In this paper, we define a new index of dynamic manipulability for humanoid biped walking to measure dynamic flexibility of changing mechanics by using residual redundancy, when primary work is being assigned, such as face and eyes being targeted to certain object. Although some measurements have been arranged so far to evaluate static or dynamical flexibility of hand manipulator. This paper displays a new measurement of Dynamic Reconfiguration Manipulability Shape Index (DRMSI) which is the combination of dynamic manipulability and reconfiguration manipulability, and we have applied the DRMSI into humanoid robot experiments to evaluate its dynamical reconfiguration ability during walking. According to the value of DRMSI in our experiments, we have verified our humanoid robot model is reliable and effective since the results have indicated that the kinematic and dynamic characteristics of our model are similar to human-being.

## I. INTRODUCTION

In the world, many researchers made their efforts to control humanoid walking and proposed many effective methods to measure walking flexibility. As we all known, ZMP-based walking motion is considered as the most effective and hopeful method, which has been certified to be a useful control tactic to perform stability of practical biped walking, because it can make sure that the humanoid can get the balance of walking and standing by keeping the ZMP within the convex hull of supporting space [1]. Nakamura [2] showed the way of representing connection between motions and environment combining the dynamical equation of motion and put into execution on human. Since dimension number of biped walking dynamical states is variable by contacting conditions of foot with floor, we need some measurements that discuss continually kinematic or dynamical flexibility of humanoid according to the bipedal gaits' variety.

The behavior of human's walking seems to use redundancy during undertaking a prior task of biped walking or eyes staring. Thus, we are willing to talk about dynamical redundancy of humanoid biped walking in this paper, proposing the concept of dynamical reconfiguration manipulability Shape Index (DRMSI), which evaluates flexibility and stability of a dynamical system which can possibly produce a motion in a workspace with standardized input torque, which is the combination of the dynamic manipulability (DM) [7] with reconfiguration manipulability (RM) [8]. The new index evaluates the flexibility of the dynamical system of humanoid robots and possesses the ability of shape-changing acceleration in workspace using unit torque input for all joints

<sup>1</sup>Keli Shen is with Division of Mechanical and Systems Engineering, Graduate school of Natural Science and Technology Okayama University, 1-1-1 Tsushima-naka, Kita-ku, Okayama 700-8530, Japan pue85qr6@s.okayama-u.ac.jp

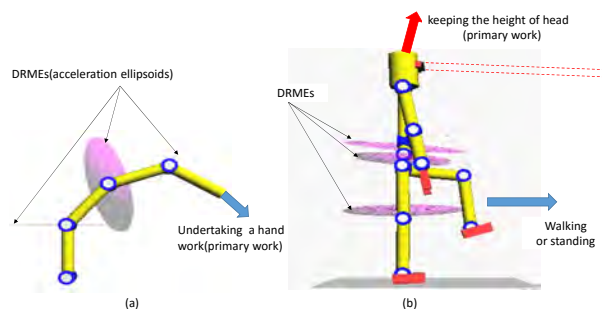


Fig. 1. Applications of DRME for (a) redundant manipulator and (b) humanoid robot.

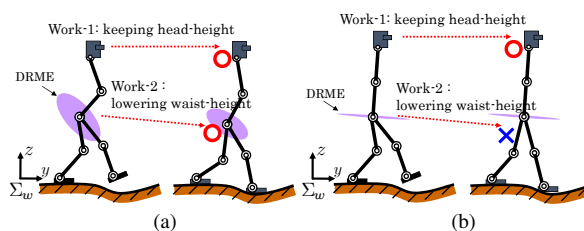


Fig. 2. Walking on uneven floor with (a) no-singular mechanics has a redundancy to accelerate the waist position during keeping head posture and making the foot reach the uneven floor (b) partially singular mechanics (from waist to head) has no ability to keep the current head posture, during the foot reaching floor. This result can be analyzed by the DRME, indicating the width in z-axis is nearly zero and ellipse shape is flat.

during undertaking prior work. We have applied DRMSI to a humanoid robot, whose primary work is assigned to keep head position or orientation close to desired one as much as possible. The concept is shown in Fig. 1(b) and the Dynamic Reconfiguration Manipulability Ellipsoid (DRME) of floor-fixed four link robot is shown in Fig. 1(a), and we think that ellipsoid also includes ellipse and line segment in this paper. Simulations showed the value of DRME was relative to the change of the human's waist height, indicating that index can be useful such as the case that the whole shape-change control can be improved through DRME based on request of secondary work different from walking. We can also conclude that our new humanoid robot model is valid and has the similar motion characteristics like human-being.

Walking on the uneven floor is shown in Fig. 2. Considering condition of work-1 (keeping the height of head) and work-2 (lowering the height of waist) is set. These work give an assumption that humanoid's face and eyes should be targeted to certain object during walking on the uneven floor. There is space for z-acceleration of waist in (a), which enable robot to undertake work-1 and work-2 simultaneously at the



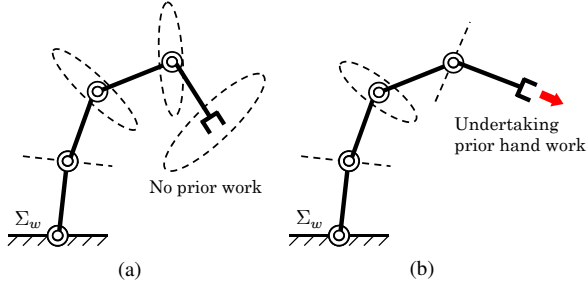


Fig. 5. (a) Dynamic manipulability ellipsoids (DMEs)(no prior work) and (b) dynamic reconfiguration manipulability ellipsoids (DRMEs) (undertaking prior work).

where  $M(\mathbf{q}) \in R^{n \times n}$  represents inertia matrix,  $\mathbf{h}(\mathbf{q}, \dot{\mathbf{q}}) \in R^n$  and  $\mathbf{g}(\mathbf{q}) \in R^n$  represent vectors of Coriolis force, centrifugal force and gravity,  $\mathbf{D} = \text{diag}[d_1, d_2, \dots, d_n]$  is matrix representing coefficients of joints' viscous friction and  $\boldsymbol{\tau} \in R^n$  represents joint torque. The kinematic equation of manipulators, the relation between the  $j$ -th link's velocity  $\dot{\mathbf{r}}_j \in R^m$  and the angular velocity  $\dot{\mathbf{q}} \in R^n$  is described by

$$\dot{\mathbf{r}}_j = \mathbf{J}_j \dot{\mathbf{q}} \quad (j = 1, 2, \dots, n). \quad (4)$$

Then,  $\mathbf{J}_j \in R^{m \times n}$  can be described as Jacobian matrix including zero block matrix,  $\mathbf{J}_j = [\tilde{\mathbf{J}}_j, \mathbf{0}]$ . Through differentiating calculation of (4), we can achieve (5)

$$\ddot{\mathbf{r}}_j = \mathbf{J}_j(\mathbf{q})\ddot{\mathbf{q}} + \dot{\mathbf{J}}_j(\mathbf{q})\dot{\mathbf{q}} \quad (5)$$

where  $\dot{\mathbf{J}}_j(\mathbf{q})\dot{\mathbf{q}}$  represents the acceleration rooted in nonlinear-relation of two-coordinates-space from  $\mathbf{q}_j$  to  $\mathbf{r}_j$ . Then, we can obtain (6) from (3) and (5)

$$\ddot{\mathbf{r}}_j - \dot{\mathbf{J}}_j \dot{\mathbf{q}} = \mathbf{J}_j \mathbf{M}^{-1} [\boldsymbol{\tau} - \mathbf{h}(\mathbf{q}, \dot{\mathbf{q}}) - \mathbf{g}(\mathbf{q}) - \mathbf{D} \dot{\mathbf{q}}]. \quad (6)$$

Here, two variables are defined as follows:

$$\tilde{\boldsymbol{\tau}} \triangleq \boldsymbol{\tau} - \mathbf{h}(\mathbf{q}, \dot{\mathbf{q}}) - \mathbf{g}(\mathbf{q}) - \mathbf{D} \dot{\mathbf{q}} \quad (7)$$

$$\ddot{\tilde{\mathbf{r}}}_j \triangleq \ddot{\mathbf{r}}_j - \dot{\mathbf{J}}_j \dot{\mathbf{q}} = \mathbf{J}_j \ddot{\mathbf{q}}. \quad (8)$$

Then, (6) can be rewritten as

$$\ddot{\tilde{\mathbf{r}}}_j = \mathbf{J}_j \mathbf{M}^{-1} \tilde{\boldsymbol{\tau}} \quad (j = 1, 2, \dots, n). \quad (9)$$

Considering serial desired accelerations  $\ddot{\tilde{\mathbf{r}}}_j$  of all links being producible by serial joint torques  $\tilde{\boldsymbol{\tau}}_j$  satisfying an Euclidean norm condition ( $\|\tilde{\boldsymbol{\tau}}_j\| = (\tilde{\tau}_1^2 + \tilde{\tau}_2^2 + \dots + \tilde{\tau}_j^2)^{1/2} \leq 1$ ), and then the each front end acceleration makes an ellipsoid in range room of  $\mathbf{J}_j$ . These ellipsoids of each link have been known as "Dynamic Manipulability Ellipsoid (DME)" from [7] (Fig. 5(a)) which are denoted in (10).

$$\tilde{\boldsymbol{\tau}}_j^T (\mathbf{J}_j (\mathbf{M}^T \mathbf{M})^{-1} \mathbf{J}_j^T)^+ \tilde{\boldsymbol{\tau}}_j \leq 1, \quad \text{and} \quad \tilde{\boldsymbol{\tau}}_j \in R(\mathbf{J}_j) \quad (10)$$

where,  $R(\mathbf{J}_j)$  represents range room of  $\mathbf{J}_j$ .

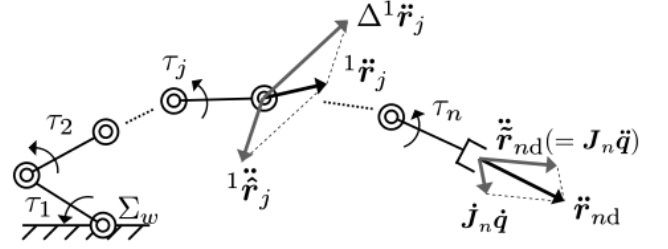


Fig. 6. Configuration change of intermediate links during manipulator executing work.

### B. Dynamic Reconfiguration Manipulability

Here, the desired end-effector's acceleration  $\ddot{\mathbf{r}}_{nd}$  is considered as prior work. Putting  $j = n$  into (9), the desired  $\ddot{\tilde{\mathbf{r}}}_j$  is described by  $\ddot{\tilde{\mathbf{r}}}_{nd}$ ,

$$\ddot{\tilde{\mathbf{r}}}_{nd} = \mathbf{J}_n \mathbf{M}^{-1} \tilde{\boldsymbol{\tau}}. \quad (11)$$

From (11),  $\tilde{\boldsymbol{\tau}}$  is obtained in (12)

$$\tilde{\boldsymbol{\tau}} = (\mathbf{J}_n \mathbf{M}^{-1})^+ \ddot{\tilde{\mathbf{r}}}_{nd} + [\mathbf{I}_n - (\mathbf{J}_n \mathbf{M}^{-1})^+ (\mathbf{J}_n \mathbf{M}^{-1})] \mathbf{l} \quad (12)$$

where,  $\mathbf{l}$  represents an arbitrary vector which satisfies  $\mathbf{l} \in R^n$ . The left superscript "1" of  $\mathbf{l}$  represents the first dynamic configuration change subtask. In the right side of (12), the first part describes the solution of minimizing  $\tilde{\boldsymbol{\tau}}$  in the null room of  $\mathbf{J}_n \mathbf{M}^{-1}$  during executing  $\ddot{\tilde{\mathbf{r}}}_{nd}$ .

The second part describes the elements of torques at each joint, which can change the configuration of manipulator despite of the influence of arbitrary  $\ddot{\tilde{\mathbf{r}}}_{nd}$  as end-effector acceleration for trailing the desired path. In this research,  $\mathbf{l}$  is commanded by a higher-level dynamic reconfiguration control system and  $\mathbf{l}$  can be used for ordinary dynamic configuration change subtask.

The relation between  $\mathbf{l}$  and  $\ddot{\tilde{\mathbf{r}}}_{nd}$  is described in (13) by substituting (12) into  $\mathbf{l} = \mathbf{J}_j \mathbf{M}^{-1} \tilde{\boldsymbol{\tau}}$

$$\mathbf{l} = \mathbf{J}_j \mathbf{M}^{-1} (\mathbf{J}_n \mathbf{M}^{-1})^+ \ddot{\tilde{\mathbf{r}}}_{nd} + \mathbf{J}_j \mathbf{M}^{-1} [\mathbf{I}_n - (\mathbf{J}_n \mathbf{M}^{-1})^+ (\mathbf{J}_n \mathbf{M}^{-1})] \mathbf{l}. \quad (13)$$

Here, two new variables are defined in the following equations

$$\Delta^1 \ddot{\tilde{\mathbf{r}}}_{jd} \triangleq \mathbf{l} - \mathbf{J}_j \mathbf{M}^{-1} (\mathbf{J}_n \mathbf{M}^{-1})^+ \ddot{\tilde{\mathbf{r}}}_{nd} \quad (14)$$

$${}^1 \boldsymbol{\Lambda}_j \triangleq \mathbf{J}_j \mathbf{M}^{-1} [\mathbf{I}_n - (\mathbf{J}_n \mathbf{M}^{-1})^+ (\mathbf{J}_n \mathbf{M}^{-1})]. \quad (15)$$

In (14),  $\Delta^1 \ddot{\tilde{\mathbf{r}}}_{jd}$  is named after "the first dynamic configuration change acceleration." In (15),  ${}^1 \boldsymbol{\Lambda}_j$  is a  $m \times n$  matrix named after "the first dynamic configuration change matrix." And then, (13) can be simplified as

$$\Delta^1 \ddot{\tilde{\mathbf{r}}}_{jd} = {}^1 \boldsymbol{\Lambda}_j \mathbf{l}. \quad (16)$$

The relation between  $\mathbf{l}$  and  $\Delta^1 \ddot{\tilde{\mathbf{r}}}_{jd}$  is shown in Fig. 6. However, the key is how to find out  $\mathbf{l}$  to generate  $\Delta^1 \ddot{\tilde{\mathbf{r}}}_{jd}$ . Solving  $\mathbf{l}$  in (16) as

$${}^1l = {}^1\Lambda_j^+ \Delta^1 \ddot{r}_{jd} + (\mathbf{I}_n - {}^1\Lambda_i^+ {}^1\Lambda_j)^2 l. \quad (17)$$

In (17),  ${}^2l$  is an arbitrary vector which satisfies  ${}^2l \in R^n$ .  ${}^1l$  is assumed to consist with restricted condition  $\|{}^1l\| \leq 1$ , and then next equation is obtained,

$$\Delta^1 \ddot{r}_{jd}^T ({}^1\Lambda_j^+)^T {}^1\Lambda_j^+ \Delta^1 \ddot{r}_{jd} \leq 1. \quad (18)$$

If  $\text{rank}({}^1\Lambda_i) = m$ , (18) denotes an  $m$ -dimensional room ellipsoid, satisfying

$$\Delta^1 \ddot{r}_{jd} = {}^1\Lambda_j^+ \Delta^1 \ddot{r}_{jd}, \quad \Delta^1 \ddot{r}_{jd} \in R^m, \quad (19)$$

which means that  $\Delta^1 \ddot{r}_{jd}$  can be arbitrarily obtained in  $m$ -dimensional room and (18) always has the value  ${}^1l$  satisfying all  $\Delta^1 \ddot{r}_{jd} \in R^m$ . Besides, if  $\text{rank}({}^1\Lambda_j) = p < m$ ,  $\Delta^1 \ddot{r}_{jd}$  is not obtained arbitrarily in  $R^m$ . Thus, we name reduced  $\Delta^1 \ddot{r}_{jd}$  after  $\Delta^1 \ddot{r}_{jd}^*$ . Then (18) can be denoted as the following equation, which is proposed by [9]

$$\begin{aligned} (\Delta^1 \ddot{r}_{jd}^*)^T ({}^1\Lambda_j^+)^T {}^1\Lambda_j^+ \Delta^1 \ddot{r}_{jd}^* &\leq 1 \\ (\Delta^1 \ddot{r}_{jd}^* = {}^1\Lambda_j^+ \Delta^1 \ddot{r}_{jd}^*). \end{aligned} \quad (20)$$

Equation (20) denotes an  $r$ -dimensional room ellipsoid. These ellipsoid described in (18) and (20) are shown in Fig.5(b). Therefore, if the matrix  $\Lambda$  conducted by the singular value dissolution, we can get

$${}^1\Lambda_j = {}^1U_j^1 \Sigma_j^1 V_j^T \quad (21)$$

$${}^1\Sigma_j = \begin{matrix} & r & & n-r \\ r & \begin{bmatrix} {}^1\sigma_{j,1} & & & 0 \\ & \ddots & & \\ & & {}^1\sigma_{j,r} & \\ m-r & & & 0 \end{bmatrix} & & \end{matrix} \quad (22)$$

In (21) and (22),  ${}^1U \in R^{m \times m}$ ,  ${}^1V \in R^{n \times n}$  denote orthogonal matrixes, and  $r$  is the number of non-zero singular values of  ${}^1\Lambda_j$  ( $\sigma_{j,1} \geq \dots \geq \sigma_{j,r} > 0$ ). Besides,  $r \leq m$  since  $\text{rank}({}^1\Lambda_j) \leq m$ . Thus, when the end-effector of manipulator executes some work, dynamic configuration change flexibility of  $j$ -th link can be denoted as

$${}^1w_j = {}^1\sigma_{j,1} \cdot {}^1\sigma_{j,2} \cdots {}^1\sigma_{j,r}. \quad (23)$$

In this paper, we name the value of  $w_j$  in (23) after dynamic reconfiguration manipulability measure (DRMM), indicating the degree of that configuration change acceleration of  $j$ -th link can be obtained from different direction. And then, volume of dynamic configuration change ellipsoid at the  $j$ -th link is defined as

$${}^1V_{DRj} = c_m \cdot {}^1w_j \quad (24)$$

$$c_m = \begin{cases} 2(2\pi)^{(m-1)/2} / [1 \cdot 3 \cdots (m-2)m] & (m : \text{odd}) \\ (2\pi)^{m/2} / [2 \cdot 4 \cdots (m-2)m] & (m : \text{even}) \end{cases} \quad (25)$$

For taking dynamic reconfiguration measure of the whole manipulator-links into consideration, we give an indicatrix

called dynamic reconfiguration manipulability shape index (DRMSI):

$${}^1W_{DR} = \sum_{j=1}^{n-1} a_j {}^1V_{DRj}. \quad (26)$$

In this paper, singular-values are enlarged a hundredfold to obtain formal value of ellipsoid, comparing with ellipse or line segment. For robots in sagittal plane like Fig. 5(b),  $a_j$  is denoted as

$$a_1 = a_{n-1} = 1[m^{-1}], \quad a_{2,3,\dots,(n-2)} = 1[m^{-2}]. \quad (27)$$

## V. APPLICATION TO HUMANOID BIPED ROBOT BASED ON DRMSI

This section is aimed at using the measurement tool to analyze the flexibility of biped walking. Firstly, keep the height of the head and assume the constraint condition  $\|{}^1l\| \leq 1$ , DRMEs are plotted in Fig. 7. There are 8 ellipses generating on the tip of the links. The volume of ellipse is formed by the manipulability to judge the mobility performance of biped walking links. Here, DRMEs are determined by  ${}^1\Lambda_j$ , which depends on both the jacobian matrix and the inertial matrix in the (15). Furthermore, two variables mentioned above are actually the functions about humanoid joint angles from the supporting foot to the head. Therefore, DRMEs are actually dominated by joint angles. In other words, DRMEs are determined by the configuration of biped walking robot. Combining the shape of ellipse in Fig. 7 and the equation (22), (23), (24), we can find that ellipse area is composed of the lines representing the all the accelerations producing potentially in the different directions of whole or part workspace. In (22),  ${}^1\sigma_{j,1}, {}^1\sigma_{j,2}$  correspond to the macro axis and minor axis, representing the biggest acceleration and the smallest acceleration. In general, the micro axis denotes the desired acceleration. In Fig. 7 (a), 4 ellipses in the neck, shoulders and waist locate in the X-Y plane, there is the desired acceleration in the direction Y axis, which means robot will go along the direction of Y axis potentially. This is due to humanoid leg can only rotate in the Y-Z plane, robot has the inertial tendency of forwarding the direction of Y axis. On the other hand, in Fig. 7 (b), 4 ellipses in the waist, hip and supporting leg locate in the Y-Z plane, there is also the desired acceleration in the direction Y axis. 8 ellipses of biped humanoid have the same potential forwarding performance, indicating the harmony of the biped walking. And then, we calculate all the joint reconfiguration flexibility with (26) from the supporting foot to the head (except the head ellipsoid since keeping the height of the head is prior task). The value of DRMSI is the total of the calculated joint acceleration while obtaining the optimal walking configuration by adjusting the joint angles.

And then, biped walking is simulated on the even ground. In this section, we use the visual-lifting method mentioned in section 3. Here, we change the  $\mathbf{K}_p$  to control the joint torque  $\tau_h(t)$  in (2) from the supporting foot to the head to overcome the gravity and the influence of walking dynamics, assuming there is an upward force keeping

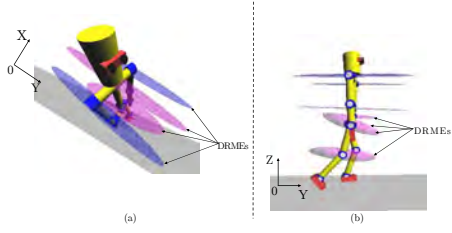


Fig. 7. The DRMEs of biped walking humanoid

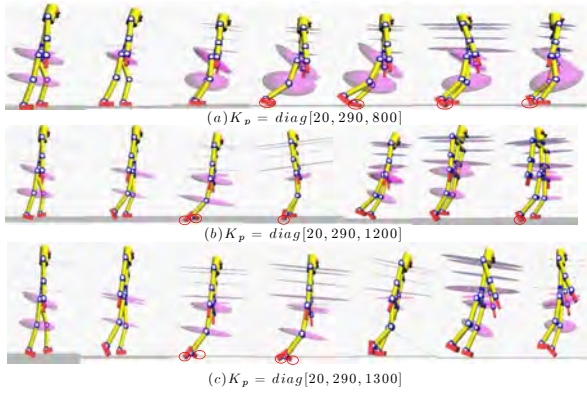


Fig. 8. Screen-shot of unstably biped walking with DRMEs about different gain sets

the height of the head directly. To begin with, we should determine the range of lifting-proportional-gain to realize the biped walking general safety and stability on the even ground. And then, we performed some simulations to obtain the suitable range, finding that under the conditions of (a)  $\mathbf{K}_p = \text{diag}[20, 290, 800]$ , (b)  $\mathbf{K}_p = \text{diag}[20, 290, 1200]$ , and (c)  $\mathbf{K}_p = \text{diag}[20, 290, 1300]$ , humanoid robot can not walking stably shown in Fig. 8. The red marks on the foots indicate gaits have collision with the floor since the float foot can not leave ground resulting in constraints out of work. So we set five sorts of lifting-proportional-gain, such as (a)  $\mathbf{K}_p = \text{diag}[20, 290, 900]$ , (b)  $\mathbf{K}_p = \text{diag}[20, 290, 950]$ , (c)  $\mathbf{K}_p = \text{diag}[20, 290, 1000]$ , (d)  $\mathbf{K}_p = \text{diag}[20, 290, 1050]$  and (e)  $\mathbf{K}_p = \text{diag}[20, 290, 1100]$ , to analyze that how the different heights of waist influence the biped walking flexibility and stability according to comparing the DRMSI values corresponding to different walking gaits. Thus, in this paper, we choose the states that float foot was going to point-contact the surface of floor and become supporting-foot, which was easy to obtain and compare DRMSI shown in Fig. 9 (a)-4, (b)-4, (c)-4, (d)-4, (e)-4. In Fig. 10, the lowest point means the minimum value obtained while the gaits is like (a)-4, (b)-4, (c)-4, (d)-4, (e)-4. Comparing the minimum value, we get a conclusion that as the lifting gain become larger under the stable walking, DRMSI is obtained with the maximum corresponding to the same gait marked with the black circle in Fig. 10, which means there is an optimal configuration to keep better walking flexibility. These group of experiments indicated our humanoid robot model was correct and it had

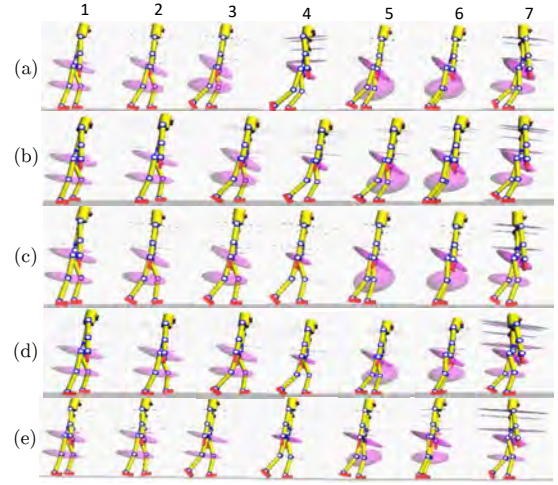


Fig. 9. Screen-shot of biped walking with DRMEs about different gain set : (a)  $\mathbf{K}_p = \text{diag}[20, 290, 900]$ , (b)  $\mathbf{K}_p = \text{diag}[20, 290, 950]$ , (c)  $\mathbf{K}_p = \text{diag}[20, 290, 1000]$ , (d)  $\mathbf{K}_p = \text{diag}[20, 290, 1050]$ , (e)  $\mathbf{K}_p = \text{diag}[20, 290, 1100]$ .

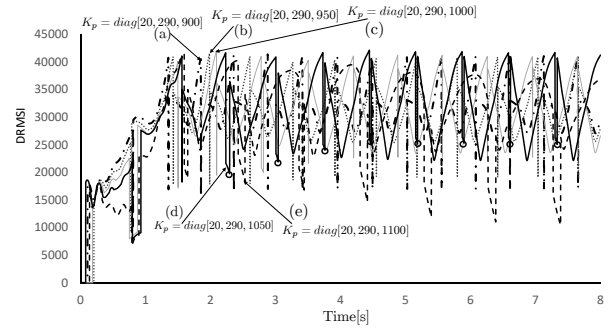


Fig. 10. DRMSI until  $t = 8.0[s]$ .

the same kinematic and dynamic performance as human-being.

Furthermore, In Fig. 11, the trajectory is designed to estimate the Dynamical Reconfiguration Manipulability of humanoid walking on the uneven ground. Besides, ladder height  $\delta h$  was set as  $0.02[m]$ ,  $0.03[m]$ ,  $0.04[m]$  to consider the influence of the change of it on DRMSI. The gain  $\mathbf{K}_p = \text{diag}[20, 290, 1000]$ , which enables humanoid robot to walk stably, were chosen to evaluate the influence of the change of ladder height on Dynamical Reconfiguration Manipulability. The value change of DRMSI was shown from Fig. 12 to Fig?14. The red mark was the value of DRMSI when humanoid robot walk down the first step.

In the case that humanoid robot walked on the uneven ground with lifting-gain  $\mathbf{K}_p = \text{diag}[20, 290, 1000]$ , if the ladder height increased, the value of DRMSI when humanoid robot walked down the first step became smaller, which was shown from Fig. 12 to Fig. 14. What we can conclude from above is that if the ladder height become larger, the Dynamical Reconfiguration Manipulability of humanoid walking down the stairs will become smaller. In other words,

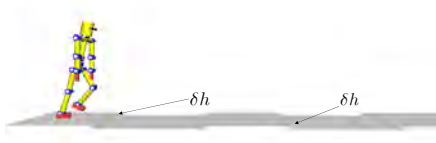


Fig. 11. The uneven ground

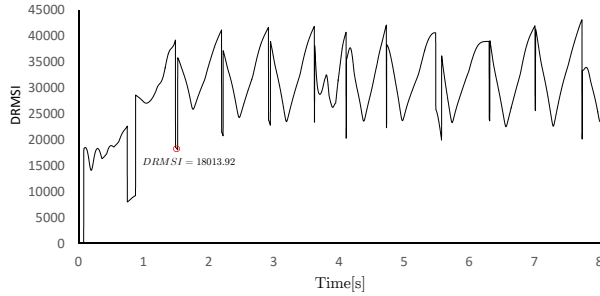


Fig. 12. Case:  $K_p = \text{diag}[20, 290, 1000]$ ,  $\delta h = 0.02[m]$

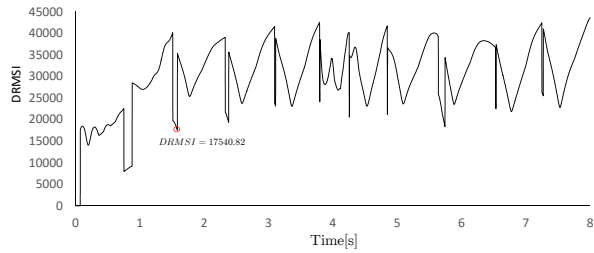


Fig. 13. Case:  $K_p = \text{diag}[20, 290, 1000]$ ,  $\delta h = 0.03[m]$

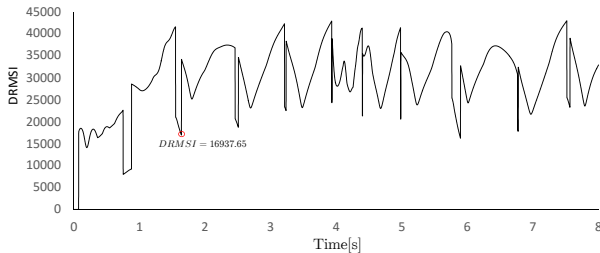


Fig. 14. Case:  $K_p = \text{diag}[20, 290, 1000]$ ,  $\delta h = 0.04[m]$

humanoid robot can walk more stably and faster on even ground than on the uneven ground. Thus, this characteristic is also like our human-being.

## VI. CONCLUSION

In this paper, we defined a new indicatrix called Dynamic Reconfiguration Manipulability Shape Index (DRMSI) for the optimization of dynamic flexibility using redundancy for reconfiguration. And DRMSI was applied to our simulation experiments of humanoid biped walking. According to changing the waist height and ladder height, we found that walking flexibility and stability were different by the value of DRMSI, which indicated that our robot model

was similar to human-being on the kinematic and dynamic characteristics such as suitable walking posture. On the other hand, we demonstrated that our new humanoid robot model was correct and effective.

## REFERENCES

- [1] M. Vukobratovic, A. Frank and D. Juricic, "On the Stability of Biped Locomotion," *IEEE Transactions on Biomedical Engineering*, Vol. 17, No. 1, 1970.
- [2] Y. Nakamura and K. Yamane, "Dynamics of Kinematic Chains with Discontinuous Changes of Constraints—Application to Human Figures that Move in Contact with the Environments—," *Journal of RSJ*, Vol. 18, No. 3, pp. 435–443, 2000 (in Japanese).
- [3] M. Kouchi, M. Mochimaru, H. Iwasawa and S. Mitani, "Anthropometric database for Japanese Population 1997-98," Japanese Industrial Standards Center (AIST, MITI), 2000.
- [4] T. Maeba, M. Minami, A. Yanou, J. Nishiguchi, "Dynamical Analyses of Humanoid's Walking by Visual Lifting Stabilization Based in Event-driven State Transition Cooperative manipulations based on Genetic Algorithms using contact information," *2012 IEEE/ASME Int. Conf. on Advanced Intelligent Mechatronics Proc.*, pp. 7–14, 2012.
- [5] W. Song, M. Minami, F. Yu, Y. Zhang and A. Yanou, "3-D Hand & Eye-Vergence Approaching Visual Servoing with Lyapunov-Stable Pose Tracking," *Proceedings of IEEE International Conference on Robotics and Automation*, pp. 5210–5217, 2011.
- [6] F. Yu, W. Song and M. Minami, "Visual Servoing with Quick Eye-Vergence to Enhance Trackability and Stability," *Proceedings of IEEE/RSJ International Conference on Intelligent Robots and Systems*, pp. 6228–6233, 2010.
- [7] T. Yoshikawa, "Dynamic Manipulability of Robot Manipulators," *Proceedings of the IEEE International Conference on Robotics and Automation*, Vol. 2, No. 1, pp. 113–124, 1985.
- [8] M. Minami, Y. Naitoh and T. Asakura, "Avoidance Manipulability for Redundant Manipulators," *Journal of the Robotics Society of Japan*, Vol. 17, No. 6, pp. 887–895, 1999 (in Japanese).
- [9] M. Minami, X. Li, T. Matsuno and A. Yanou, "Dynamic Reconfiguration Manipulability for Redundant Manipulators," *Journal of the Mechanisms Robotics*, Vol. 8 / 061004-1- 061004-9, 2016.
- [10] Y. Kobayashi, M. Minami, A. Yanou and T. Maeba "Dynamic Reconfiguration Manipulability Analyses of Humanoid Bipedal Walking," *Proceedings of the IEEE International Conference on Robotics and Automation (ICRA)*, , pp. 4764-4769, 2013.